THE JOURNAL OF PHYSICAL CHEMISTRY C

Article

pubs.acs.org/JPCC

Ethylenediamine-Enhanced Oxidation Resistivity of a Copper Surface during Water-Based Copper Nanowire Synthesis

Jahyun Koo,[†] Soonho Kwon,[†] Na Rae Kim, Kihyun Shin, and Hyuck Mo Lee*

Department of Materials Science and Engineering, KAIST, 291 Daehak-ro, Yuseong-gu, Daejeon 34141, Republic of Korea

Supporting Information

ABSTRACT: Copper nanowires (Cu NWs) are promising materials for transparent electrode applications. However, their growth mechanism during water-based synthesis remains unclear. The steric hindrance of a surfactant, which has been considered in previous studies, is insufficient to explain the suppression of Cu oxide formation during water-based synthesis. In this paper, we suggest that ethylenediamine (EDA, $C_2H_4(NH_2)_2$), which is commonly used as a structure-directing agent (SDA), may play an important role as an oxidation inhibitor in water-based synthesis of Cu NWs. High-resolution transmission electron microscopy (HR-TEM) analysis indicated that the Cu NWs grow from icosahedral seeds. Additionally, energy-dispersive X-ray spectroscopy (EDS) and X-ray photoelectron spectroscopy (XPS) suggested that EDA affects the oxidation state of the as-prepared Cu NW surface. Finally, density functional theory (DFT) calculations revealed that the adsorption of EDA effectively hinders the adsorption of oxidizing species and prevents the oxidation of the Cu seeds. This effect is attributed to a filling of the antibonding states and an increase in the electrostatic repulsion between the Cu seeds and the oxidizing species.

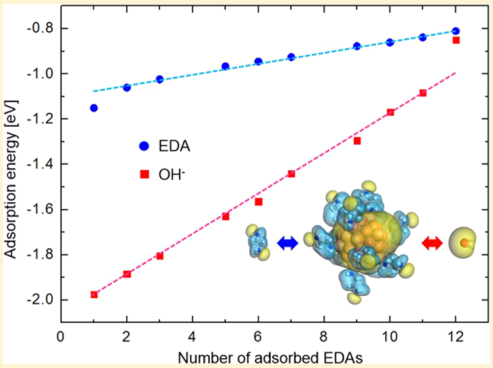

INTRODUCTION

Indium tin oxide (ITO) is extensively used in optoelectronic devices. However, ITO is an expensive material because of resource limitations. The U.S. Geological Survey has reported that the demand for indium has significantly increased in China.[1] The price of indium has also continuously increased. In addition, the manufacturing of ITO requires vacuum, etching, and evaporation processes to coat substrates. Recently, potential alternatives to ITO, such as carbon nanotubes,[2] graphene,[3] metal nanowires (NWs),[4,5] and graphene/metal NW hybrids,[6] have been investigated. Among these materials, metal NWs exhibit a low sheet resistance and flexibility, which is advantageous for flexible and transparent applications. Currently, silver nanowires (Ag NWs)[5] and copper nanowires (Cu NWs)[7−10] are considered to be promising materials for use in flexible transparent conductive films, organic solar cells, and organic light-emitting diodes.[4] Although the oxidative properties of Cu NWs remain problematic, studies of Cu NWs have increased because of their low cost and high conductivity.[9,11]

Previously, Cu NWs were grown through various methods, including chemical vapor deposition,[12] electrospinning,[8] and wet processes (polyol and water-based synthesis).[10,13] Among these methods, water-based synthesis has many advantages because it is highly scalable and does not require a vacuum process. Water-based synthesis was first reported by Chang and Rathmell.[11,13] However, Cu NWs have a unique head and body structure compared with that of simple one-dimensional (1D) NWs synthesized by other methods. A decahedron seed induces simple 1D NWs in a typical polyol process but does not do so in the water-based synthesis. However, the type of seed that drives the distinctive head and body structure of Cu NWs in water-based synthesis remains unknown. Meng and Jin have investigated the novel growth mechanism of Cu NWs in water-based synthesis and have reported that screw dislocations induce Cu NW growth.[14] Many dislocation sources able to initiate NW growth have been observed in the intersection between the seed and the body. However, Meng and Jin did not describe the unique head−body structure of the Cu NWs formed via water-based synthesis.

The amine functional group has been used as a structure-directing agent (SDA) to grow Cu NWs in polyol and water-based syntheses.[9−11] This SDA possesses preferential capping characteristics for anisotropic nanostructure synthesis processes.[15,16] However, Ye et al. have recently suggested that ethylenediamine (EDA), which is used as an SDA in water-based synthesis, suppresses the nucleation of copper oxide (Cu_2O) nanoparticles (NPs).[17] However, the oxidation-inhibition mechanisms have not been previously discussed. Many oxidizing species are present during water-based synthesis, such as water molecules, hydroxide ions, and dissolved oxygen (O). Therefore, the potential role of EDA in preventing Cu_2O formation during this synthesis may be important for understanding the growth mechanism of Cu NWs.

Received: November 3, 2015
Revised: January 27, 2016
Published: February 1, 2016

DOI: 10.1021/acs.jpcc.5b10733
J. Phys. Chem. C 2016, 120, 3334−3340

One strategy for enhancing oxidation resistivity involves the use of a capping agent to prevent the diffusion of the oxidizing species. The oxidation resistivity enhancement attributed to steric hindrance has been previously explored using experimental[18−20] and theoretical approaches.[21] However, the short molecular length of EDA (~4 Å) is insufficient to effectively block the oxidizing species' access to the Cu NWs. In addition, the Cu precursor (dihydroxycopper(I), ($Cu(OH)_2^-$)[22]) is much larger in size than the oxidizing species, and the amount of oxidizing species present is much higher than that of EDA or the Cu precursor. Therefore, steric hindrance from EDA is insufficient to explain the suppression of Cu_2O NP formation during Cu NW synthesis. In this respect, we expected that the oxidation resistivity enhancement of NPs is caused not only by kinetic factors, i.e., steric hindrance, but also by energetic factors. Thus, we performed a DFT study to elucidate the electronic energy contribution. Here, we explored the role of EDA as an oxidation inhibitor protecting Cu seed NPs. We propose the formation of an icosahedron-like Cu seed structure early in the water-based Cu NW synthesis on the basis of high-resolution transmission electron microscopy (HR-TEM) analysis. The experimental results were used to design an icosahedral Cu NP for use in density functional theory (DFT) calculations. The DFT results revealed the energetic effect of EDA on the adsorption of the oxidizing species.

EXPERIMENTAL SECTION

Synthesis of Cu NWs. We slightly modified the previously reported Cu NW synthesis procedure.[13] Cu nitrate (Sigma-Aldrich, 12837) was used as the Cu precursor, EDA (Sigma-Aldrich, E1521) was used as the SDA, and hydrazine (35 wt %, Sigma-Aldrich, 309400) was used as the reducing agent. Cu nitrate (0.16 g), sodium hydroxide (NaOH, 48 g), and deionized water (80 mL) were mixed for 2 min prior to heating to 60 °C in a silicon oil bath for 30 min with stirring to equilibrate the reaction temperature. Next, EDA (0.1−0.6 mL, 1.3−8 mmol) and hydrazine (0.2 mL) were sequentially added dropwise to the solution, and the resulting solution was held in the oil bath for 2 min. Next, the solution was placed in a plastic tube in an oven at 30 °C for 1−2 h to grow homogeneous Cu NWs. The resulting Cu NWs floated on the surface of the solution.

Preparation for Scanning Electron Microscopy (SEM), Tunneling Electron Microscopy (TEM), and X-ray Photoelectron Spectroscopy (XPS) Analyses. The floating Cu NWs were removed and placed in a centrifuge tube containing a 3 wt % hydrazine washing solution. The resulting solution was centrifuged twice at 2000 rpm for 10 min. Next, the washed Cu NWs were centrifuged twice in ethanol at 2000 rpm for 10 min. The Cu NWs were dispersed in ethanol and deposited onto sample grids for SEM (FEI Company, USA, Nova 230), TEM (FEI Company, USA, Technai TF30 ST), focused ion beam (FIB) (FEI Company, USA, Helios Nanolab 450 F1), and XPS (Thermo VG Scientific Co. Ltd., USA, K-alpha) analyses.

Computational Details. The DFT calculations were conducted using the DMol^3 code.[23] The generalized gradient approximation (GGA) was used to determine the exchange-correlated interactions with the Perdew and Wang (PW91) functional.[24] In addition, double numerical basis sets with dynamic nuclear polarization (DNP) functions were used, and the nuclei and core electrons were described using DFT semilocal pseudopotentials.[25] The geometries were optimized until the forces that acted on each ion core were less than 0.004 Ha/Å without any symmetry constraints. The electronic structures were relaxed with a convergence tolerance of 2.0×10^{-5} Ha. The presence of solvent was considered using the "conductor-like screening model" (COSMO),[26] especially for hydroxide ion (OH^-) hydration.[27] The adsorption energy (E_{ads}) of an adsorbate was defined as

$$E_{ads} = E_{adsorbate/NP} - E_{NP} - E_{adsorbate} \quad (1)$$

where $E_{adsorbate/NP}$ is the system energy of an adsorbate on the Cu NP, E_{NP} is the system energy of a single Cu NP, and $E_{adsorbate}$ is the energy of an adsorbate.

RESULTS AND DISCUSSION

Cu NWs were obtained through water-based synthesis at approximately 60−80 °C, as described by other researchers.[9−11] First, we synthesized Cu NWs in aqueous solutions (48 g of NaOH and 80 mL of deionized [DI] water) with EDA (0.3 mL, 4 mmol) at 60 °C (Figure 1a). The length and thickness of the obtained Cu NWs were 20 μm and 200 nm, respectively. However, the Cu heads were round because of the burst nucleation and growth (Figure 1b). The Cu head structure was difficult to recognize, even under magnification.

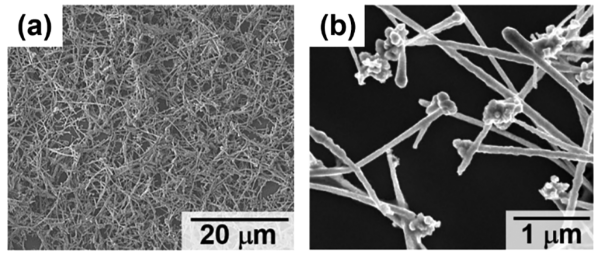

Figure 1. (a) SEM image of the Cu particles synthesized at 60 °C with 4 mmol of EDA and (b) a magnified SEM image of the same Cu particles.

To investigate the Cu head structure, we divided the Cu NW reaction into two steps: nucleation and growth. First, the Cu seeds were synthesized at 60 °C. Second, the Cu NWs were grown at 30 °C. In the second step, we retarded the growth to afford the crystalline Cu head structure (Figure 2 and Figure S1). Cu NPs were observed only with the use of hydrazine (reducing agent) and in the absence of EDA (Figure 2a). Cu rods or Cu NWs were obtained when we added EDA to the synthesis (Figure 2b−d). As the EDA concentration increased, well-dispersed Cu NWs were obtained. When the EDA concentration was 4 mmol, thin NWs with lengths ranging from 10 to 30 μm and thicknesses ranging from 50 to 150 nm were observed (Figure 2c).

A representative Cu NW head exhibiting the unique facets is shown in Figure S1. This type of Cu NW has been previously observed.[9,11,17,28] However, none of the relevant studies have described the origin of this characteristic Cu NW structure. Unfortunately, the formation of this type of NW was difficult to explain relative to the traditional NW growth model.[7,15,16] In the traditional growth mechanism, decahedron seeds are commonly used to explain NW growth.[29,30] The decahedra have pentagonal[31] or round[32] cross sections, and the NWs grow in two opposite [110] directions on the penta-twinned surfaces of the decahedral seed without a distinguishable head. However, our Cu NWs exhibited a distinguishable head, and the rest of the structure resembled a body. Therefore, other types of seeds and growth mechanisms are required because the

DOI: 10.1021/acs.jpcc.5b10733
J. Phys. Chem. C 2016, 120, 3334−3340

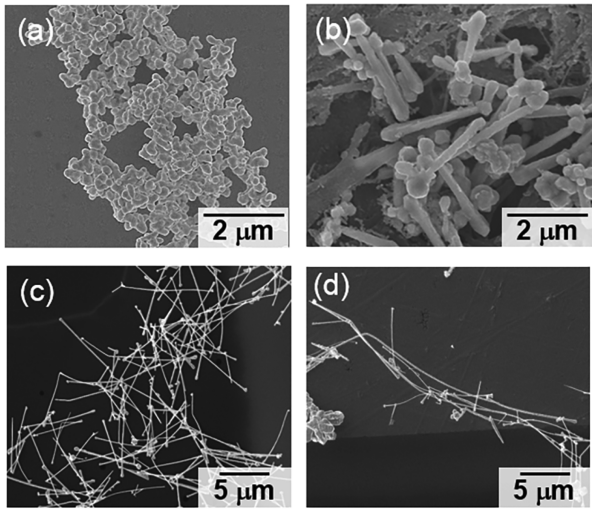

Figure 2. SEM image of the Cu particles synthesized in two steps (60 → 30 °C): (a) without EDA, (b) with 1.33 mmol of EDA, (c) with 4 mmol of EDA, and (d) with 8 mmol of EDA.

shape of the anisotropic nanostructure is highly dependent on the seed morphology.

The Cu seed structure was investigated using experiments and DFT calculations. First, we observed a single Cu NW synthesized using 4 mmol (0.3 mL) of EDA (Figure 3a). In this

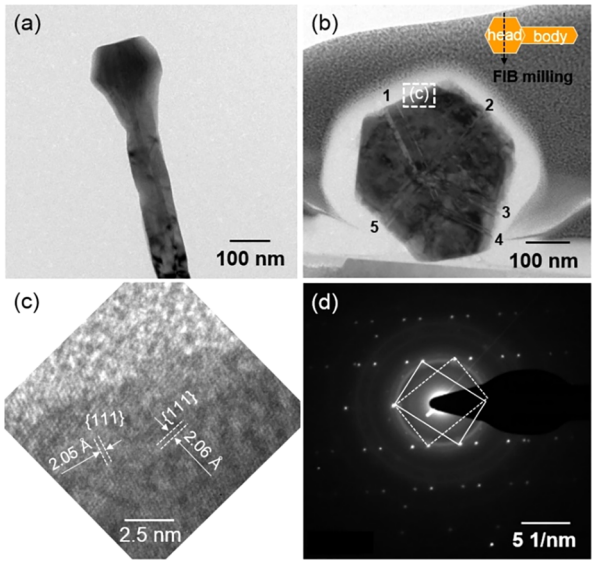

Figure 3. (a) TEM image of a Cu NW synthesized with 4 mmol (0.3 mL) of EDA. (b) TEM image of the cross section of the head portion of the Cu NW prepared by FIB ion milling. The hexagonal character of the cross section and the existence of a 5-fold twinned structure implies that the seed of the Cu NWs is an icosahedron. (c) HR-TEM image of the head of the Cu NW. (d) SAED pattern of the cross section, which shows the twinned structure of the head.

case, the head and body of the Cu NW were distinguishable in the TEM image. We cut the head of the Cu NW perpendicular to the horizontal axis by using FIB milling. The cut image revealed that the seed had five twinned boundaries (Figure 3b). In addition, the HR-TEM image indicated that the Cu atoms were stacked on the (111) surfaces (Figure 3c). The icosahedron and decahedron geometrically consisted of (111) surfaces. In addition, the selected area electron diffraction (SAED) pattern indicated that the Cu seed structure was twinned (Figure 3d). Therefore, icosahedron and decahedron were among the candidate structures, and perfect crystal structures (i.e., cubic, octahedron, and tetrahedron) were excluded.[33] However, a decahedron seed could not generate the head and body structure observed because it grows into a simple 1D structure. In addition, the cross section of the Cu NW head was hexagonally shaped,[34,35] corresponding to the preferential facet shape. These observations provided evidence for an icosahedron-like seed. To obtain more information about the head and body structure, we cut a Cu NW perpendicular to the vertical axis (Figure S2). The head part of the Cu NW had a well-organized crystal structure (Figure S2a,b). The body part of the Cu NW had a [110] growth direction with (111) Cu atom stacked layers (Figure S2c,d). The horizontally cross-sectioned body also showed 5-fold symmetry (Figure S3). The body part extended through decahedron-like 1D growth. However, the intersection between the head and body parts (Figure S2e,f) indicated that they are connected to each other without a large mismatch. Therefore, the alternative seed structure is an icosahedron with 5-fold symmetric twins that extend from a central NP hub and a hexagonal projection shape.[31,36] Second, to confirm the experimental observation, the total energies of the icosahedron, decahedron, and cuboctahedron of N Cu atoms (N = 13, 55, and 147) were calculated using DFT calculations. The results show that the icosahedron had lower energy than the decahedron and cuboctahedron (Table S1). These results indicated that the icosahedron is thermodynamically more stable than the decahedron and cuboctahedron.

To confirm the role of EDA as an oxidation inhibitor, the oxidation layer was analyzed using XPS in samples grown with various EDA concentrations. The oxidation state of the Cu NW surface was analyzed as a function of the EDA concentration. The EDA concentration ranged from 1.3 to 8 mmol, and a copper precursor concentration of 0.8 mmol was used to compare the surface oxidation levels. At an EDA concentration of 1.3 mmol (a low concentration of EDA), the amount of EDA was insufficient to prevent the oxidation of the Cu seeds, thus resulting in anisotropic growth during the synthesis. However, longer and thinner Cu NWs were formed in the solution that contained 4 mmol of EDA (a moderate concentration of EDA), thus indicating that the Cu precursor required at least a five-to-one ratio of EDA to grow suitable NWs.

The oxidation trend as a function of the EDA concentration was investigated using XPS. The spectra were referenced to the adventitious C 1s with a binding energy of 284.6 eV.[37,38] The XPS spectra were fitted using Gaussian curves. The Cu $2p_{3/2}$ peaks and O 1s peaks are shown in Figures 4a and 4b, respectively. In Figure 4, Cu^0 exhibited a single peak at 932.3 eV[39] with a full width at half-maximum (fwhm) of 1.3 ± 0.2 eV (peak 1), and Cu^{2+} exhibited a peak at 933.6 eV[37,38] (peak 2) with a fwhm of 3.5 eV[37] and satellite peaks at higher energies (peaks 3 and 4). The copper(II) oxide (CuO) composition (peak 2) relative to the metallic copper (peak 1) on the surface decreased as the EDA concentration increased (from peak 2 to peak 2′). Peaks 3 and 4 appeared in the samples obtained with 4 mmol of EDA and 5.33 mmol of EDA, respectively. However, the CuO satellite peaks (peaks 3 and 4) nearly disappeared when the EDA concentration increased to 6.67 mmol. The O 1s main peak (peak 6) was located at 530.9 eV, as shown in Figure 4b.[40] The peaks of the metal oxides were primarily observed to the right of the main peak. The CuO peak (peak 5)

DOI: 10.1021/acs.jpcc.5b10733
J. Phys. Chem. C 2016, 120, 3334−3340

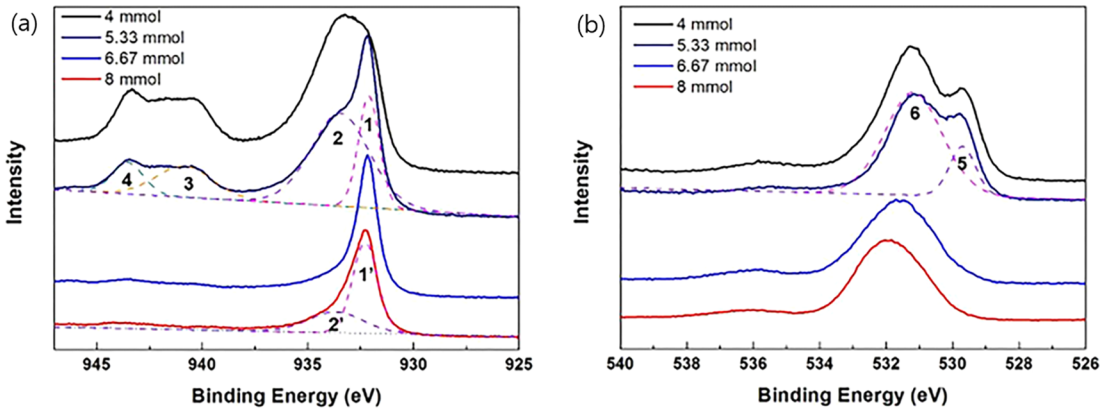

Figure 4. XPS spectra of the (a) Cu $2p_{3/2}$ and (b) O 1s states of the Cu NWs synthesized with different EDA concentrations.

was located at 529.2 eV[41] and disappeared in the sample obtained with 6.67 mmol of EDA, thus indicating that EDA behaved as an oxidation inhibitor in the solution. EDA generally prevented oxidation of the Cu NWs. The elemental analysis indicated that EDA affected the interactions between the Cu surfaces and the O sources.

To elucidate how EDA functions as an oxidation inhibitor during the synthesis, DFT calculations were performed. Based on computational costs, a Cu_{55} icosahedron structure was used as the Cu NP model. In addition to the use of a bare Cu NP, the binding nature of EDA as an SDA for Cu NW synthesis was investigated. The amine group preferentially forms a single bond with a Cu atom on the surface because the amine group has one lone pair of electrons. Therefore, EDA adsorbs onto one of two different sites on the surface of the Cu NPs (Figure S4). The adsorption energies of EDA were −1.15 eV at the vertex and −0.934 eV at the edge. Therefore, EDA energetically prefers vertex sites (Figure 5a). The partial charges were calculated using a Mulliken population analysis before and after EDA adsorption to investigate the electronic interactions between EDA and the Cu NPs. The calculated atomic charges for the single Cu NP and the adsorbed system are summarized in Table 1. These interactions did not vary when the number of adsorbed EDA molecules was changed (Figure S5). In the single-Cu NP system, the electrons were concentrated in the shell of the Cu NP. When EDA absorbed onto the Cu NP, 0.35 electrons were transferred from the EDA molecule to the Cu NP shell. However, the charges on the core atoms were not significantly altered because most of the electrons were transferred to the Cu NP shell. In addition, the increase in the total charge of the shell atoms suggested that the transferred electrons possess a delocalized character. Thus, a single EDA molecule can affect the chemical activity of the entire Cu NP surface. Next, the Cu NP adsorption energies of adsorbates containing oxygen atoms were calculated to estimate the oxidation resistivity. Water molecules (H_2O) and OH^- ions were used as the oxygen sources because of their natural abundance in the synthesis solution. The DFT results indicated that the adsorption energy of OH^- on the Cu NPs (−2.09 eV) was substantially higher than that of H_2O on the Cu NPs (−0.43 eV). Therefore, OH^- predominantly contributes to Cu NP oxidation. The adsorption of OH^- ions on metal surfaces is an important issue.[42,43] In addition, the transformation of the metastable $Cu(OH)_2$ phase to CuO is rapid in the presence of OH^-, which implies that the formation of $Cu(OH)_2$ may be critical for the formation of Cu oxide.[44] Therefore, the adsorption of OH^- on Cu NPs can cause significant oxidation, especially in the highly basic environment of our experiment. The most stable adsorption occurred at the bridge site, which is located between the vertex site and the edge site (Figure 5b). Because the most stable adsorption sites for EDA and OH^- are different, these species adsorbed on Cu NP with little steric hindrance (Figure 5c). During the adsorption of an OH^- ion, 0.69 electrons were transferred from OH^- to the Cu NP, which is more than 2 times greater than in the EDA case. In addition,

Table 1. Mulliken Partial Charges of the System before and after the Adsorption of EDA and OH^- [a]

EDA adsorption	before	after	OH^- adsorption	before	after
Cu NP shell	−1.43	−1.76	Cu NP shell	−1.43	−2.13
Cu NP core	1.43	1.42	Cu NP core	1.43	1.44
EDA	0	0.35	OH^-	−1.00	−0.31

[a]Both EDA and OH^- primarily donate electrons to the Cu NP shell atoms.

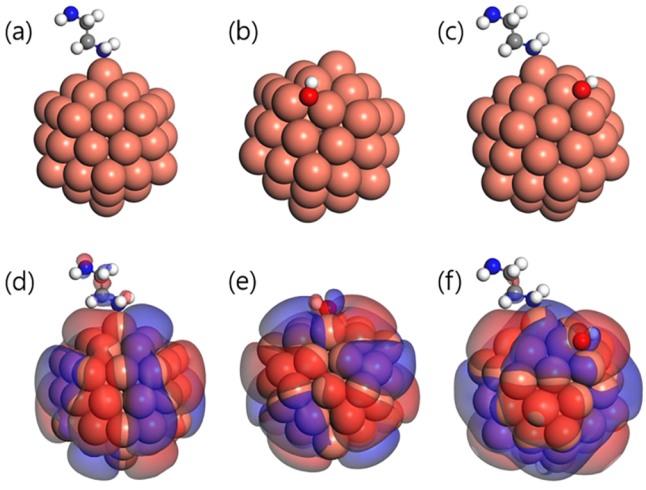

Figure 5. Optimized geometry of the (a) Cu NP-EDA, (b) Cu NP-OH^-, and (c) Cu NP-EDA-OH^- systems. The orange, blue, gray, red, and white atoms correspond to Cu atoms, N atoms, C atoms, O atoms, and H atoms, respectively. The preferred adsorption sites of EDA and OH^- are the vertex and bridge sites, respectively. The HOMOs of the (d) Cu NP-EDA, (e) Cu NP-OH^-, and (f) Cu NP-EDA-OH^- systems are shown. The systems' HOMOs indicate antibonding between the Cu NPs and adsorbates.

DOI: 10.1021/acs.jpcc.5b10733
J. Phys. Chem. C 2016, 120, 3334−3340

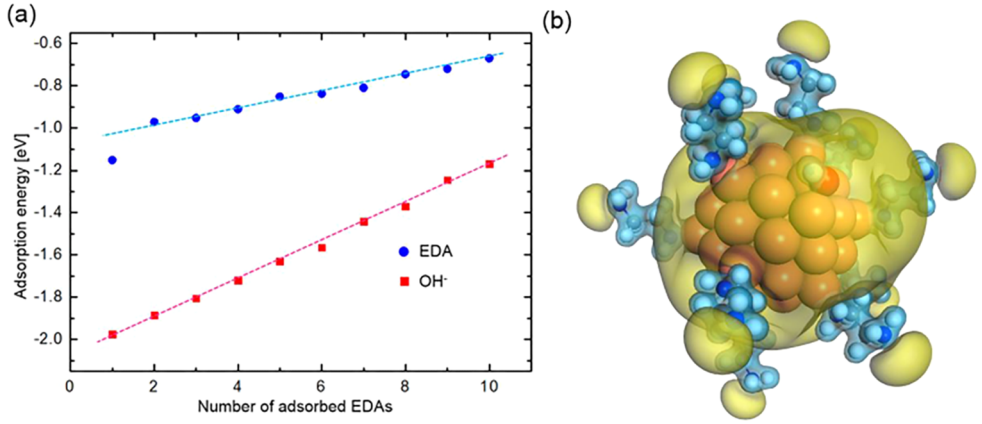

Figure 6. (a) Linear relationships between the adsorption energy of the adsorbates and the number of adsorbed EDA molecules indicating that the adsorption of additional EDA molecules can hinder OH^- adsorption. (b) The isosurface of the electrostatic potential. The light-blue and yellow regions represent the positive and negative potentials, respectively.

the adsorption energy of the OH^- ions was twice the adsorption energy of EDA.

To determine the relationship between the oxidation resistivity of the Cu NPs and the EDA concentration, the adsorption energy of OH^- on the Cu NPs was calculated in the presence of various amounts of EDA molecules adsorbed on the NP. The calculated energies for OH^- and EDA are shown in Figure 6a. The adsorption energies of OH^- linearly decreased as the number of EDA molecules increased. These results imply that the adsorption of EDA energetically disrupts the adsorption of OH^-, which is a major source of oxygen in the reaction solution. In addition, a linear change in the adsorption energy of OH^- on the Cu NP with the number of adsorbed EDA molecules occurred regardless of the relative distance between OH^- and EDA. This finding implied the absence of direct interactions between OH^- and EDA and the delocalized character of the electrons transferred from EDA to the Cu NP (as previously described). The molecular orbitals of the system were investigated to determine both adsorption energies, which decreased as a function of the number of additional adsorbed EDA molecules. The highest occupied molecular orbitals (HOMOs) of both the EDA-Cu NP and OH^--Cu NP systems exhibited antibonding character (as shown in Figures 5d,e). Because EDA and OH^- form antibonding states at the HOMO level, the electron transferred from EDA occupied the antibonding states between the Cu NP and other adsorbates (Figure 5f). In our calculations, the bond orders between the oxygen atom of OH^- and the adjacent vertex and edge of Cu atoms decreased from 0.3126 and 0.3125 to 0.2900 and 0.2884, respectively, when ten EDA molecules were adsorbed on the Cu NP. In addition, the O−Cu (vertex) and O−Cu (edge) bond lengths increased from 1.992 and 2.016 Å to 2.018 and 2.056 Å, respectively.

The decrease in the OH^- adsorption energy was significantly steeper than the decrease in the EDA adsorption energy as the number of EDA molecules increases (Figure 6a). Although the EDA adsorption energy decreased by 0.431 eV for the adsorption of the 10th EDA molecule, the OH^- adsorption energy decreased by 0.805 eV when ten EDA molecules were adsorbed on the Cu NP. Although the adsorption energy of OH^- was initially larger than the adsorption energy of EDA, a reversal in the adsorption energy of OH^- and EDA on the Cu NPs may occur when high concentrations of EDA are added. The EDA concentration was significantly higher than the concentration of the Cu precursor in the solution. The bigger decrease in the adsorption energy of OH^- can be explained by the electrostatic interactions that occur between the adsorbates and the Cu NP. Previously, Preuss et al.[45] have reported that Coulomb interactions are the main driving force for bonding between the amino groups and the Cu surface. In contrast to OH^-, which has a negatively charged O, EDA is positively charged after adsorption (Figure 6b). Because the Cu NP became more negatively charged with increasing EDA adsorption, the electrostatic attraction between EDA and the Cu NP and the electrostatic repulsion between OH^- and the Cu NP increased. Therefore, the decrease in the OH^- adsorption energy was significantly larger than the decrease in the EDA adsorption energy.

CONCLUSIONS

On the basis of the HR-TEM analysis, we propose the use of a Cu icosahedron-like structure as a seed for growing Cu NWs. The relationship between the EDA concentration and the oxidation of the Cu NWs was investigated using XPS analysis. When an icosahedron model was used, the results from the DFT study indicated that ligands enhance the oxidation resistivity of Cu NPs by energetically preventing the adsorption of OH^- ions, which are the main oxidizing species in the synthesis solution. In our calculations, the adsorption of ten EDA molecules decreased the OH^- adsorption energy by 0.8 eV. This decrease was caused by the filling of the antibonding states and increasing the electrostatic repulsion between the Cu seed and the oxidizing species.

ASSOCIATED CONTENT

Supporting Information

The Supporting Information is available free of charge on the ACS Publications website at DOI: 10.1021/acs.jpcc.5b10733.

SEM images of Cu heads with 4 mmol of EDA (Figure S1); TEM images of a Cu NW after FIB ion milling (Figures S2 and S3); adsorption sites on the Cu_{55} NP (Figure S4); Mulliken charges of EDA and OH- molecules as a function of EDA coverage (Figure S5); relative energies of the decahedron and cuboctahedron compared to that of the icosahedron (Table S1) (PDF)

DOI: 10.1021/acs.jpcc.5b10733
J. Phys. Chem. C 2016, 120, 3334−3340

AUTHOR INFORMATION

Corresponding Author

*E-mail: hmlee@kaist.ac.kr (H.M.L.).

Author Contributions

†Jahyun Koo and Soonho Kwon contributed equally.

Notes

The authors declare no competing financial interest.

ACKNOWLEDGMENTS

This research was supported by a National Research Foundation of Korea (NRF) grant funded by the Ministry of Science, ICT & Future Planning (MSIP) (no. NRF-2015R1A5A1037627) and by the NLRL (National Leading Research Laboratory) program of the Korea government (no. 2011-0028612).

REFERENCES

(1) Summaries Mineral Commodity, US Department of the Interior. US Geological Survey, 2015.

(2) Maillaud, L.; Poulin, P.; Pasquali, M.; Zakri, C. Effect of the Rheological Properties of Carbon Nanotube Dispersions on the Processing and Properties of Transparent Conductive Electrodes. *Langmuir* **2015**, *31*, 5928−5934.

(3) Kobayashi, T.; Bando, M.; Kimura, N.; Shimizu, K.; Kadono, K.; Umezu, N.; Miyahara, K.; Hayazaki, S.; Nagai, S.; Mizuguchi, Y.; et al. Production of a 100-m-Long High-Quality Graphene Transparent Conductive Film by Roll-to-Roll Chemical Vapor Deposition and Transfer D Process. *Appl. Phys. Lett.* **2013**, *102*, 023112.

(4) Chen, Z.; Ye, S.; Stewart, I. E.; Wiley, B. J. Copper Nanowire Networks with Transparent Oxide Shells That Prevent Oxidation without Reducing Transmittance. *ACS Nano* **2014**, *8*, 9673−9679.

(5) Hu, L.; Kim, H. S.; Lee, J.-Y.; Peumans, P.; Cui, Y. Scalable Coating and Properties of Transparent, Flexible, Silver Nanowire Electrodes. *ACS Nano* **2010**, *4*, 2955−2963.

(6) Deng, B.; Hsu, P.-C.; Chen, G.; Chandrashekar, B. N.; Liao, L.; Ayitimuda, Z.; Wu, J.; Guo, Y.; Lin, L.; Zhou, Y.; et al. Roll-to-Roll Encapsulation of Metal Nanowires between Graphene and Plastic Substrate for High-Performance Flexible Transparent Electrodes. *Nano Lett.* **2015**, *15*, 4206−4213.

(7) Zhang, D.; Wang, R.; Wen, M.; Weng, D.; Cui, X.; Sun, J.; Li, H.; Lu, Y. Synthesis of Ultralong Copper Nanowires for High-Performance Transparent Electrodes. *J. Am. Chem. Soc.* **2012**, *134*, 14283−14286.

(8) Wu, H.; Hu, L.; Rowell, M. W.; Kong, D.; Cha, J. J.; McDonough, J. R.; Zhu, J.; Yang, Y.; McGehee, M. D.; Cui, Y. Electrospun Metal Nanofiber Webs as High-Performance Transparent Electrode. *Nano Lett.* **2010**, *10*, 4242−4248.

(9) Rathmell, A. R.; Bergin, S. M.; Hua, Y.-L.; Li, Z.-Y.; Wiley, B. J. The Growth Mechanism of Copper Nanowires and Their Properties in Flexible, Transparent Conducting Films. *Adv. Mater.* **2010**, *22*, 3558−3563.

(10) Mohl, M.; Pusztai, P.; Kukovecz, A.; Konya, Z.; Kukkola, J.; Kordas, K.; Vajtai, R.; Ajayan, P. M. Low-Temperature Large-Scale Synthesis and Electrical Testing of Ultralong Copper Nanowires. *Langmuir* **2010**, *26*, 16496−16502.

(11) Rathmell, A. R.; Wiley, B. J. The Synthesis and Coating of Long, Thin Copper Nanowires to Make Flexible, Transparent Conducting Films on Plastic Substrates. *Adv. Mater.* **2011**, *23*, 4798−4803.

(12) Zaraska, L.; Sulka, G. D.; Jaskuła, M. Fabrication of Free-Standing Copper Foils Covered with Highly-Ordered Copper Nanowire Arrays. *Appl. Surf. Sci.* **2012**, *258*, 7781−7786.

(13) Chang, Y.; Lye, M. L.; Zeng, H. C. Large-Scale Synthesis of High-Quality Ultralong Copper Nanowires. *Langmuir* **2005**, *21*, 3746−3748.

(14) Meng, F.; Jin, S. The Solution Growth of Copper Nanowires and Nanotubes is Driven by Screw Dislocations. *Nano Lett.* **2012**, *12*, 234−239.

(15) Sun, Y.; Mayers, B.; Herricks, T.; Xia, Y. Polyol Synthesis of Uniform Silver Nanowires: A Plausible Growth Mechanism and the Supporting Evidence. *Nano Lett.* **2003**, *3*, 955−960.

(16) Yang, H.-J.; He, S.-Y.; Tuan, H.-Y. Self-Seeded Growth of Five-Fold Twinned Copper Nanowires: Mechanistic Study, Characterization, and SERS Applications. *Langmuir* **2014**, *30*, 602−610.

(17) Ye, S.; Rathmell, A. R.; Ha, Y.-C.; Wilson, A. R.; Wiley, B. J. The Role of Cuprous Oxide Seeds in the One-Pot and Seeded Syntheses of Copper Nanowires. *Small* **2014**, *10*, 1771−1778.

(18) Kanninen, P.; Johans, C.; Merta, J.; Kontturi, K. Influence of Ligand Structure on the Stability and Oxidation of Copper Nanoparticles. *J. Colloid Interface Sci.* **2008**, *318*, 88−95.

(19) Yuping, B.; Michael, B.; Alexandre, B. P.; Kannan, M. K. Controlled Crystalline Structure and Surface Stability of Cobalt Nanocrystals. *J. Phys. Chem. B* **2005**, *109*, 7220−7222.

(20) Nguyet, D.; Kyösti, K.; Christoffer, J. Directing Oxidation of Cobalt Nanoparticles with the Capping Ligand. *J. Colloid Interface Sci.* **2010**, *350*, 126−131.

(21) Alnemrat, S.; Hooper, J. P. Oxidation of Ligand-Protected Aluminum Clusters: An ab Initio Molecular Dynamics Study. *J. Chem. Phys.* **2014**, *140*, 104313.

(22) Ye, S.; Chen, Z.; Ha, Y.-C.; Wiley, B. J. Real-Time Visualization of Diffusion-Controlled Nanowire Growth in Solution. *Nano Lett.* **2014**, *14*, 4671−4676.

(23) Delley, B. An All-Electron Numerical Method for Solving the Local Density Functional for Polyatomic Molecules. *J. Chem. Phys.* **1990**, *92*, 508−517.

(24) Perdew, J. P. Generalized Gradient Approximations for Exchange and Correlation: A Look Backward and Forward. *Phys. B* **1991**, *172*, 1−6.

(25) Delley, B. Hardness Conserving Semilocal Pseudopotentials. *Phys. Rev. B: Condens. Matter Mater. Phys.* **2002**, *66*, 155125.

(26) Delley, B. The Conductor-Like Screening Model for Polymers and Surfaces. *Mol. Simul.* **2006**, *32*, 117−123.

(27) Nechaev, I. V.; Vvedenskii, A. V. Quantum Chemical Modeling of Hydroxide Ion Adsorption on Group IB Metals from Aqueous Solutions. *Prot. Met. Phys. Chem. Surf.* **2009**, *45*, 391−397.

(28) Han, S.; Hong, S.; Ham, J.; Yeo, J.; Lee, J.; Kang, B.; Lee, P.; Kwon, J.; Lee, S. S.; Yang, M.-Y.; et al. Fast Plasmonic Laser Nanowelding for a Cu-Nanowire Percolation Network for Flexible Transparent Conductors and Stretchable Electronics. *Adv. Mater.* **2014**, *26*, 5808−5814.

(29) Lupu, N. *Nanowires Science and Technology*; InTech: Rijeka, 2010.

(30) Pietrobon, B.; McEachran, M.; Kitaev, V. Synthesis of Size-Controlled Faceted Pentagonal Silver Nanorods with Tunable Plasmonic Properties and Self-Assembly of these Nanorods. *ACS Nano* **2009**, *3*, 21−26.

(31) Mayoral, A.; Barron, H.; Estrada-Salas, R.; Vazquez-Duran, A.; Jose-Yacaman, M. Nanoparticle Stability from the Nano to the Meso Interval. *Nanoscale* **2010**, *2*, 335−342.

(32) Narayanan, K. B.; Sakthivel, N. Green Synthesis of Biogenic Metal Nanoparticles by Terrestrial and Aquatic Phototrophic and Heterotrophic Eukaryotes and Biocompatible Agents. *Adv. Colloid Interface Sci.* **2011**, *169*, 59−79.

(33) Xia, Y.; Xiong, Y.; Lim, B.; Skrabalak, S. E. Shape-Controlled Synthesis of Metal Nanocrystals: Simple Chemistry Meets Complex Physics? *Angew. Chem., Int. Ed.* **2009**, *48*, 60−103.

(34) Leong, G. J.; Ebnonnasir, A.; Schulze, M. C.; Strand, M. B.; Ngo, C.; Maloney, D.; Frisco, S. L.; Dinh, H. N.; Pivovar, B.; Gilmer, G. H.; et al. Shape-Directional Growth of Pt and Pd Nanoparticles. *Nanoscale* **2014**, *6*, 11364−11371.

(35) Mariscal, M. M.; Velazquez-Salazar, J. J.; Yacaman, M. J. Growth Mechanism of Nanoparticles: Theoretical Calculations and Experimental Results. *CrystEngComm* **2012**, *14*, 544−549.

DOI: 10.1021/acs.jpcc.5b10733
J. Phys. Chem. C 2016, 120, 3334−3340

(36) Zhou, W.; Wu, J.; Yang, H. Highly Uniform Platinum Icosahedra Made by Hot Injection-Assisted GRAILS Method. *Nano Lett.* **2013**, *13*, 2870−2874.
(37) Wu, C.-K.; Yin, M.; O'Brien, S.; Koberstein, J. T. Quantitative Analysis of Copper Oxide Nanoparticle Composition and Structure by X-ray Photoelectron Spectroscopy. *Chem. Mater.* **2006**, *18*, 6054−6058.
(38) Tobin, J. P.; Hirschwald, W.; Cunningham, J. XPS and XAES Studies of Transient Enhancement of Cu at CuO Surfaces during Vacuum Outgassing. *Appl. Surf. Sci.* **1983**, *16*, 441−452.
(39) Ghijsen, J.; Tjeng, L. H.; Van Elp, J.; Eskes, H.; Westerink, J.; Sawatzky, G. A.; Czyzyk, M. T. Electronic Structure of Cuprous and Cupric Oxides. *Phys. Rev. B: Condens. Matter Mater. Phys.* **1988**, *38*, 11322−11330.
(40) Moulder, J. F.; Stickle, W. F.; Sobol, P. E.; Bombe, K. D. *Handbook of X-Ray Photoelectron Spectroscopy*; Physical Electronics Inc.: 1992.
(41) McIntyre, N. S.; Cook, M. G. X-Ray Photoelectron Studies on Some Oxides and Hydroxides of Cobalt, Nickel, and Copper. *Anal. Chem.* **1975**, *47*, 2208−2213.
(42) Marichev, V. A. The Adsorption of Hydroxide Ions on Metals. *Electrochim. Acta* **1998**, *43*, 2203−2214.
(43) Koper, M. T. M.; van Santen, R. A. Interaction of H, O and OH with Metal Surfaces. *J. Electroanal. Chem.* **1999**, *472*, 126−136.
(44) Singh, D. P.; Ojha, A. K.; Srivastava, O. N. Synthesis of Different Cu(OH)2 and CuO (Nanowires, Rectangles, Seed-, Belt-, and Sheetlike) Nanostructures by Simple Wet Chemical Route. *J. Phys. Chem. C* **2009**, *113*, 3409−3418.
(45) Preuss, M.; Schmidt, W. G.; Bechstedt, F. Coulombic Amino Group-Metal Bonding: Adsorption of Adenine on Cu(110). *Phys. Rev. Lett.* **2005**, *94*, 236102.

DOI: 10.1021/acs.jpcc.5b10733
J. Phys. Chem. C 2016, 120, 3334−3340